Materials and Design 109 (2016) 242–250

Contents lists available at ScienceDirect

Materials and Design

journal homepage: www.elsevier.com/locate/matdes

Fast fabrication of NiO@graphene composites for supercapacitor electrodes: Combination of reduction and deposition

Xu Hui [a], Luming Qian [a], Gary Harris [b], Tongxin Wang [b,c,*], Jianfei Che [a,b,**]

[a] Key Laboratory of Soft Chemistry and Functional Materials, Ministry of Education, Nanjing University of Science and Technology, Nanjing 210014, China
[b] College of Engineering, Howard University, Washington, DC 20059, USA
[c] College of Dentistry, Howard University, Washington, DC 20059, USA

HIGHLIGHTS

- A fast fabrication method to prepare NiO@graphene composite modified electrodes for supercapacitors.
- The porous nanostructure may provide better accessibility of electrolyte and a large electrochemically active surface.
- The higher degree of GO reduction has taken place with the increasing amount of NiO/Ni in NiO/GO films.
- The highest specific capacitance of the constructed electrodes can reach 1258 F/g at a current density of 5 A/g.

GRAPHICAL ABSTRACT

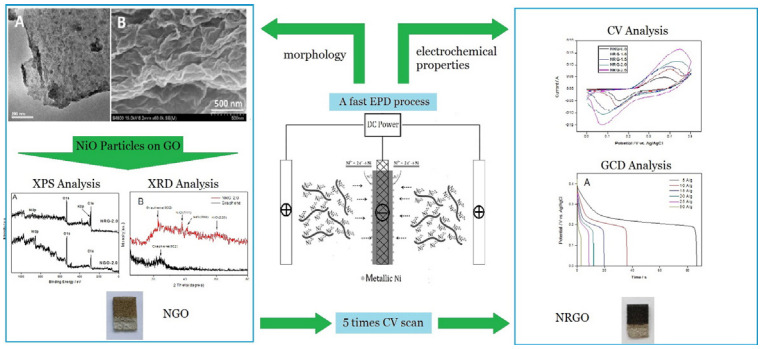

ARTICLE INFO

Article history:
Received 12 January 2016
Received in revised form 12 July 2016
Accepted 14 July 2016
Available online 15 July 2016

Keywords:
Graphene
Nickel oxide
Electrophoretic deposition
Supercapacitors

ABSTRACT

Graphene-based inorganic composites have been attracting more and more attention since the attachment of inorganic nanoparticles instead of conducting polymeric materials to graphene sheets turns out higher capacitances and good capacity retention. Here we report a fast fabrication method to prepare NiO@graphene composite modified electrodes for supercapacitors. By this method, preparation of electrochemical active materials of NiO/graphene and modification of the electrode can be simultaneously performed, which is achieved separately by traditional method. Moreover, the problem of poor adhesion of active materials on the surface of the electrode can be well solved. The NiO particles introduced to the films exhibit pseudocapacitive behavior arising from the reversible Faradaic transitions of Ni(II)/Ni(III) and greatly improve the capacitance of the electrodes. With the increase in NiO content, highly reduced graphene can be obtained during cyclic voltammetry sweeping, leading to the increase in the electrode capacitance. The highest specific capacitance of the constructed electrodes can reach 1258 F/g at a current density of 5 A/g.

1. Introduction

Supercapacitors are considered as the most important energy storage devices in future and are likely to be widely used in hybrid and electrical vehicles, portable and flexible electronics, industrial power systems and various microdevices [1–3]. However, before entering the

* Correspondence to: T. Wang, College of Engineering, Howard University, Washington, DC 20059, USA.
** Correspondence to: J. Che, Key Laboratory of Soft Chemistry and Functional Materials, Ministry of Education, Nanjing University of Science and Technology, Nanjing 210014, China.
E-mail addresses: twang@howard.edu (T. Wang), xiaoche@mail.njust.edu.cn (J. Che).

http://dx.doi.org/10.1016/j.matdes.2016.07.072
0264-1275/

commercial applications, supercapacitors still suffer from poor energy density when compared with batteries [4,5]. Searching for efficient way to improve energy density without sacrificing the power density and cycling life has yet to be achieved.

As it is shown in the energy density equation $E = 1/2\ CV^2$, the specific energy of supercapacitors can be improved by increasing the operation voltage window (V) and/or the specific capacitance (C) of the material [6,7]. Some investigations use ionic liquids or organic electrolytes to increase the operation voltage, which, however, is limited by poor ionic conductivity, high cost, short cycle life, environmental concerns, and strict fabrication conditions [6,7]. On the other hand, the specific capacitance of supercapacitors is related to two energy storage mechanisms: the electrical double-layer capacitance (EDLC) produced by charge separation and the pseudocapacitance benefited from the reversible Faradic reactions [8]. The typical materials for the electrode materials of EDLC are the classic materials of activated carbons and the recently promoted materials of carbon-based materials such as carbon fibers, carbon nanotubes and graphene, which have high specific surface area and long cycling life stability. While the electrode materials of pseudocapacitor, such as MnO_2, NiO, Co_3O_4 and conducting polymeric materials, can provide much higher energy storage capacity than the former [9]. Recently, graphene-based inorganic composites have been attracting more and more attention since the attachment of inorganic nanoparticles instead of conducting polymeric materials to the graphene sheets would lead to excellent properties. Graphene, with ultrahigh conductivity and stable physicochemical properties, has been considered as one of the most appealing conductive carbon materials. In graphene-based inorganic composites, graphene films can play a perfect role as a conductive support of inorganic oxides, while inorganic oxides can provide additional pseudocapacitance and prevent the restacking of graphene sheets during the chemical reduction process, and lead to the formation of a new class of graphene-based materials. Among the inorganic nanoparticles, NiO with its high theoretical capacitance, high thermal stability, environmentally friendly nature and abundance has been considered as one of the most promising candidates [10–12]. Nevertheless, high resistivity of pure NiO leads to low rate behavior and cycle stability, which has extremely limited its practical applications [13].

In our study, NiO/graphene composites were prepared on nickel foam via electrophoretic deposition (EPD). Of the various techniques to cast NiO/graphene films, EPD allows an efficient deposition of the composite with controlled thickness and long-range homogeneous microstructure on conductive substrates [14–16]. It has the advantages of a short processing time, simple setup, low cost, and suitability for mass production as compared with other deposition techniques. Surprisingly, when we evaluated the capacitive behavior of the electrode precursor modified with NiO/graphene oxide (GO) films using cyclic voltammetry (CV) (0 V–0.5 V, 50 mV/s) in 6 M KOH aqueous solution, a fast, unexpected color change (from yellow to black) was accompanied. Subsequent experiments revealed that GO can undergo fast deoxygenation with the deposition of metallic Ni via CV. The results indicate that deposition of NiO/graphene composite as well as chemical reduction from GO to graphene can be carried out by a fast electrochemical reaction, which aroused our significant interests in electrodeposition methods to fabricate NiO/graphene composite for the electrodes of supercapacitor. By using this method, preparation of electrochemical active materials and modification of the electrode can be simultaneously performed, which is usually achieved through a complex series of steps in traditional method. More important, the problem of poor adhesion of active materials on the surface of the electrode was well solved.

Scheme 1 illustrates the approach of preparing NiO/GO films on nickel foam by EPD. Briefly, GO sheets were exfoliated by ultrasonication in isopropyl alcohol (IPA) and were got negative charged due to the ionization of the functional groups (such as —COOH and —OH) on the GO surfaces. With $Ni(NO_3)_2$ addition, the charges on the GO surfaces reverse to positive due to the adsorption of Ni^{2+} on GO. The Ni^{2+}-decorated GO moves towards the cathode (nickel foam) by electric field force and Ni^{2+} ions bound on the GO are simultaneously reduced to form a metal of Ni. After deposition, the metallic Ni on the as-formed GO films is oxidized to NiO in the drying process and GO can undergo fast deoxygenation to graphene via CV in 6 M KOH aqueous solution. As a result, the capacitance of the NiO/graphene composite electrode is greatly improved.

2. Experimental

2.1. Electrophoretic deposition process

GO sheets were exfoliated by ultrasonication in IPA and the concentration of the suspension is about 0.5 mg/mL. To prepare a Ni^{2+}-decorated GO suspension, 2 mL as-produced GO/IPA dispersion was slowly dropped into 8 mL of $Ni(NO_3)_2$/IPA solution with a vigorous stir by vortex mixer (Vdrtex-5, Kylin-Bell Lab Instruments Co., Ltd., Haimen, China). Ni^{2+} concentrations of the suspensions are from 0.5 to 2.5 mM. Nickel foams (PPI: 120, Hanbo Environmental Protection Equipment Co., Ltd., Shenzhen, China), with a thickness of 1.6 mm, were cut into electrodes with dimensions of $1.5 \times 1\ cm^2$. These electrodes were deeply cleaned by sonication in 0.5 M H_2SO_4, acetone, DI water, ethanol, step by step, and were rinsed with ethanol prior to EPD. The EPD process was carried out at room temperature using an electrophoresis cell with 10 mL suspensions, which equipped with one negative electrode as working electrode, i.e., nickel foam, and two positive electrodes, i.e., stainless steel (Scheme 1). The area of the nickel foam immersed in the suspension was about $1 \times 1\ cm^2$. The surface area immersed in the suspension of each stainless steel electrode was 1.5 times as large as the nickel foam in order to form more uniform electric field between the electrodes. The electrodes kept parallel with a distance of 1 cm between each other. A DC voltage of 200 V (EPS-300, Tanon Science & Technology Co., Ltd.) was applied on the EPD electrodes for 10 min and thus the Ni^{2+}-decorated GO were attracted towards the nickel foam. During the EPD process, we found that when the concentration of Ni^{2+} in the suspension was lower than 0.5 mM, EPD failed due to the failure of charge conversion from negative to positive on the GO surfaces. To solve this problem, an appropriate amount of $Al(NO_3)_3$ was added into the suspension to assist the reversal of the surface charge. After EPD, all films were rinsed several times with ethanol and dried at room temperature in air. During the production or storage period, the metallic Ni on GO was oxidized to NiO to form a NiO/GO composite. The as-deposited NiO/GO electrodes from the suspensions of 0.5, 1.0, 1.5, 2.0, 2.5 mM Ni^{2+} were named as NGO-0.5 (NiO/Graphene Oxide), NGO-1.0, NGO-1.5, NGO-2.0, NGO-2.5, respectively.

Then the electrodes were performed an electrochemical reduction via CV. It was performed in a potential range of 0–0.5 V with a scan rate of 50 mV/s, using a three-electrode system (Autolab PGSTAT302N, Ecochemie, Netherlands). The as-deposited NiO/GO electrodes worked as the working electrode, a platinum wire as the counter electrode and a standard Ag/AgCl electrode as the reference electrode. The electrochemical reduction was carried out in 6 M KOH aqueous solutions for 5 times. All solutions were deaerated by bubbling nitrogen prior to experiments. After CV, the color of the electrodes changed, implying that GO can undergo fast deoxygenation to graphene in the process. The NiO@reduced graphene electrodes were renamed as NRG-0.5 (NiO/Reduced Graphene), NRG-1.0, NRG-1.5, NRG-2.0, NRG-2.5, respectively.

2.2. Characterization

The morphology of the obtained NiO/GO films was investigated by field emission scanning electron microscopy (FESEM, S-4800 II, Hitachi). X-ray photoelectron spectroscopy (XPS) were studied to analyze the surface components on the nickel foam using PHI5300 X-ray photoelectron spectrometer (PHI Quantera II system, Ulvac-PHI, INC, Japan) with monochromatic Mg Kα radiation (1253.6 eV). Raman

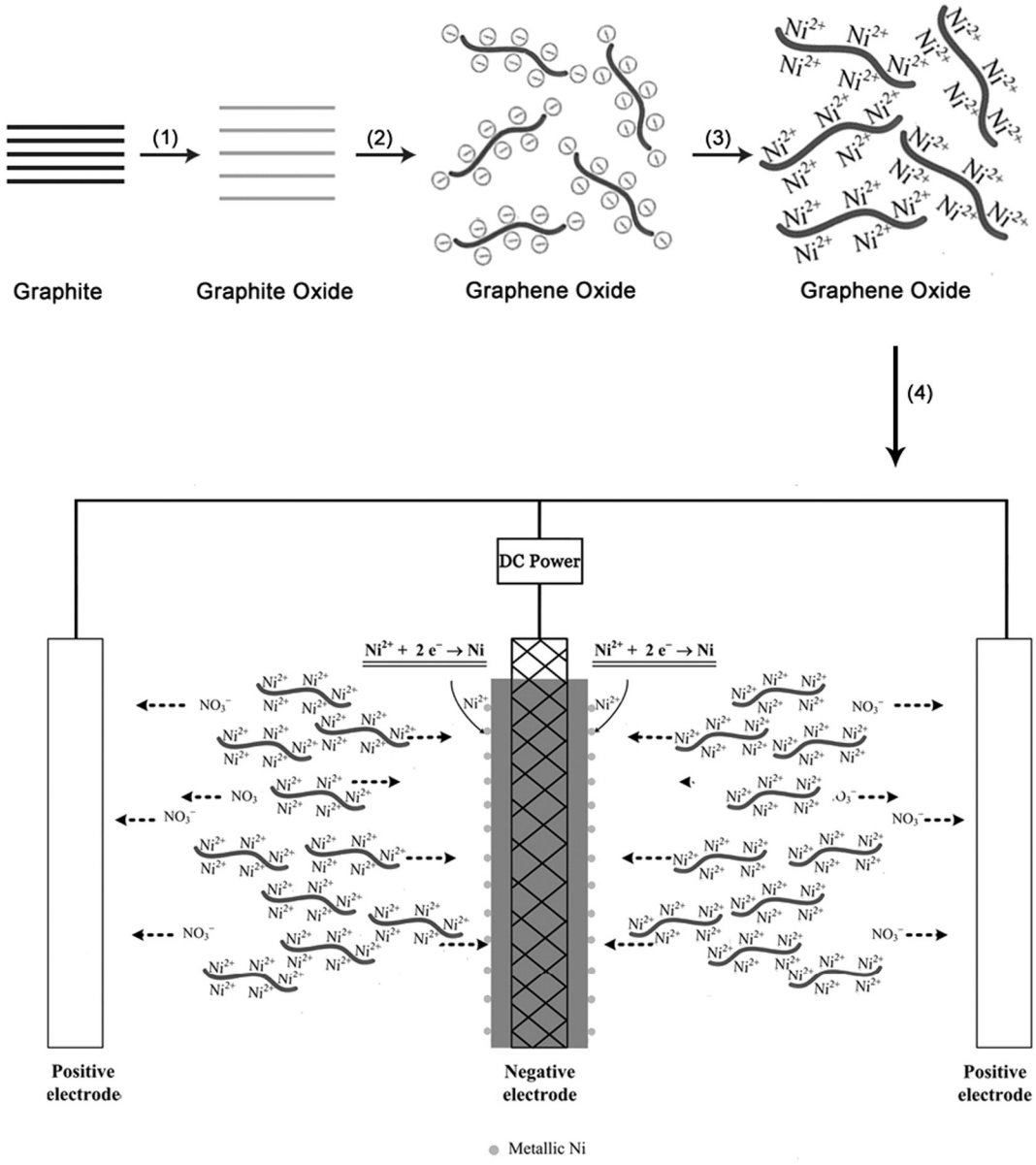

Scheme 1. Schematic diagram for the preparation of NiO/GO films on nickel foam. 1, Oxidation of graphite. 2, Exfoliation of graphite oxide. 3, Charge conversion. 4, Electrophoretic deposition.

spectra were measured on a RM2000 confocal microspectrometer (RENISHAW, Britain) with 514.5 nm Ar laser excitation. Structural properties of deposited graphene films were analyzed by X-ray diffraction (XRD) (Cu Kα radiation, λ = 0.15406 nm, Bruker AXS GmbH). The electrochemical behavior of the electrodes was analyzed using CV and galvanostatic charge/discharge in 6 M KOH electrolyte on an Autolab PGSTAT302N, where electrodes were mounted in a conventional three-electrode cell with a sample as working electrode, a standard Ag/AgCl as reference electrode and a platinum foil as counter electrode. The obtained composite electrodes were rejuvenated by CV for five times from 0 to 0.5 V before characterizations.

3. Results and discussion

EPD on the nickel foam was carried out via transport of the positively charged GO towards the cathode under the applied electric field and deposited on the electrode layer by layer. Usually GO were negative charged due to the ionization of the functional groups (such as —COOH and —OH) on the GO surfaces [17,18]. The efficiency of raw GO electrophoretic deposition is very low because of GO's low absolute potential. To solve the problem, nickel nitrate additive was added into the GO suspension to reverse GO surfaces to positive charged and significantly increase the decorated GO's absolute potential. The EPD device was composed of three electrodes so that the GO films can be acquired on both sides of the working electrode, as shown in Scheme 1.

In the EPD process, the Ni^{2+} ions bound on GO were reduced to metallic Nickel. Nickel, with its high electrical conductivity, acts as a metal binder to attach GO layer by layer. As a result, GO continued to deposit on the electrode. As indicated in the experimental section, the metallic Nickel on GO was oxidized to NiO thus form a NiO/GO composite after deposition, It was reported that different levels of initial oxidation of nickel nanoparticles occurred during the production or storage period, resulting in passivated oxide films with thickness of ca.1.0 nm [19]. The formation of the oxide on the surface of nickel nanoparticles was also confirmed by XPS and XRD in our previous work [20].

NiO/GO films were prepared from the suspensions containing different concentrations of Ni^{2+}. With the increase in Ni^{2+} content in the suspension, more and more Ni^{2+} was attached to the surface of GO and

thus electrochemically reduced to metal Ni in EPD process, followed by conversion to NiO in the subsequent drying process. Fig. 1A shows the microstructure of the nickel foam. Due to its foam-like structure (random-sized pores arranged in almost every direction in three-dimensional coordinates), Ni^{2+}-decorated GO can reach the internal of the nickel foam and deposit locally. Fig. 1B, C, D, E, F show NiO/GO films deposited from the suspensions containing different concentrations of Ni^{2+}. The surfaces of NiO/GO films exhibit a rough and wrinkled texture, a typical topography of GO, which is in association with the presence of the flexible and ultrathin GO sheets on the electrodes. However, we found that the wrinkles become increasingly blurred and even invisible from Fig. 1B to F. The phenomenon may result from the coverage of the increasing loading of NiO on the GO surface.

The coverage of NiO on the GO surface can be observed by TEM (Fig. 2A). Freestanding NiO nanoparticles are uniformly deposited onto the GO nanosheets to form a large-scale conformal coating, which can effectively prevent the self-aggregation of GO nanosheets during deposition and deoxygenation. Fig. 2B shows the cross-sectional FESEM images of NiO/GO film. The images indicate that the stacked NiO-coated GO layers present a curved and corrugated structure. Moreover, it can be observed that there are many cavities within the interlayer spaces of the NiO-coated GO films. The cavities can build porous structures for NiO/GO film and provide better accessibility of electrolyte to penetrate inside and a large electrochemically active surface to increase the capacitive performance of the electrode.

To deoxygenate GO on the electrodes, CV was performed. Fig. 3A–C shows the color change of NiO/GO electrodes before and after CV. The reduction peak appears at around 1.5 V in the first CV cycle of NGO (Fig. 3D). After five cycles of CV scan, the sample turned completely black. The obtained NiO/reduced graphene electrodes exhibit an unexpected color change, turning to homogeneous black from golden yellow (Fig. 3E). The samples before CV all present yellow and there is no obvious color change from NGO-0.5 to NGO-2.5. After the CV, the color of NRG-0.5 and NRG-1.0 was yellow-brown. Compared to NGO-0.5 and NGO-1.0, the color change was not that obvious. In contrast, the color change of the rest of the three electrodes was quite significant. The color of NRG-1.5 was brown, while the color of NRG-2.0 and NRG-2.5 was dark black. The unexpected color change implies that the reduction of GO in electrochemical reaction is carried out, the phenomenon was also observed and discussed in the reported publications [21–24]. This method of electrochemically reduction of graphene is mainly caused by the electron exchange between GO and electrodes and possesses the merit of green, fast, and higher electrochemical performance than the traditional chemical reduced graphene [25,26]. However, the production and the degree of reduction in the previous report are not comparable to that of the chemical or thermal reduction method. One of the most possible reasons is that there is lack of sufficient interface bonding between graphene and the electrodes. In our work, the reduced metallic Ni on the surface of GO, act as a conductive binder to attach GO, forms an efficient linkage between GO and electrode. Furthermore, as mentioned above, the oxidation of nickel only occurs at 1 nm depth from the surface of nickel nanoparticles at room temperature, the unoxidized nickel cores may act as reductant to help accelerate the reduction of GO. As a result, with the increasing amount of NiO/Ni in NiO/GO films, the higher degree of reduction will take place, and the higher performance of the electrode will be achieved.

In order to validate the deoxygenation, XPS analysis was carried out on the surface layer of NGO-2.0 and NRG-2.0. The peak of O1s for NRG-2.0 became relatively weak in the XPS survey scan spectra as compared with that of NGO-2.0 (Fig. 4A). In contrast, the C1s

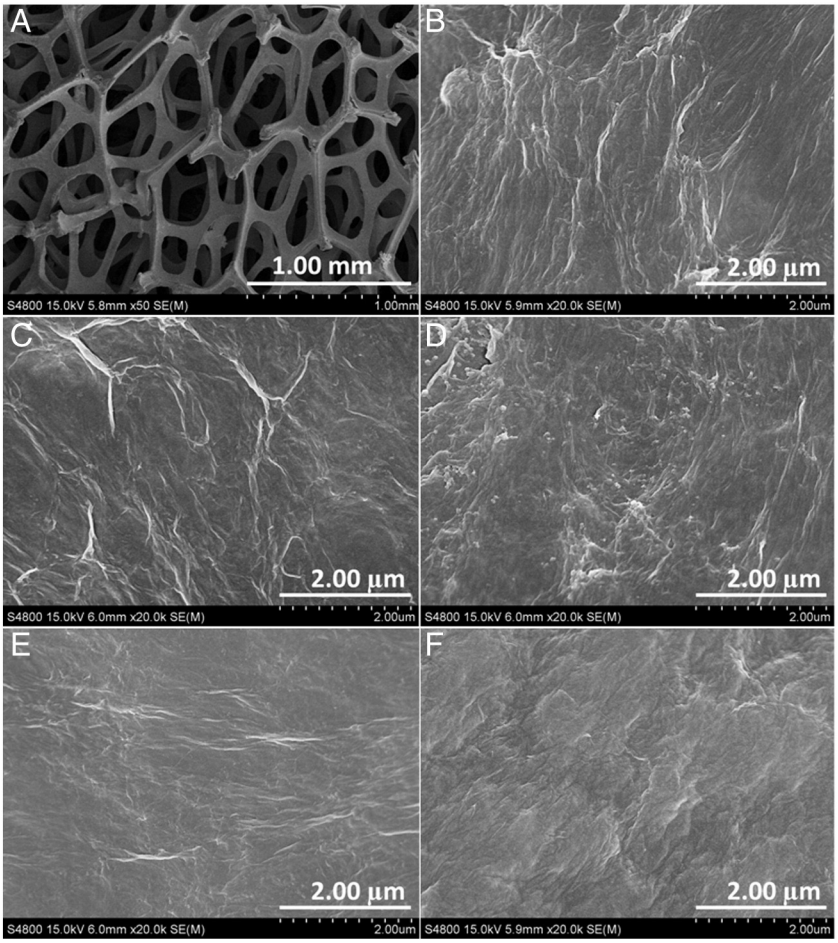

Fig. 1. FESEM images of: (A) nickel foam, (B) NGO-0.5, (C) NGO-1.0, (D) NGO-1.5, (E) NGO-2.0, (F) NGO-2.5.

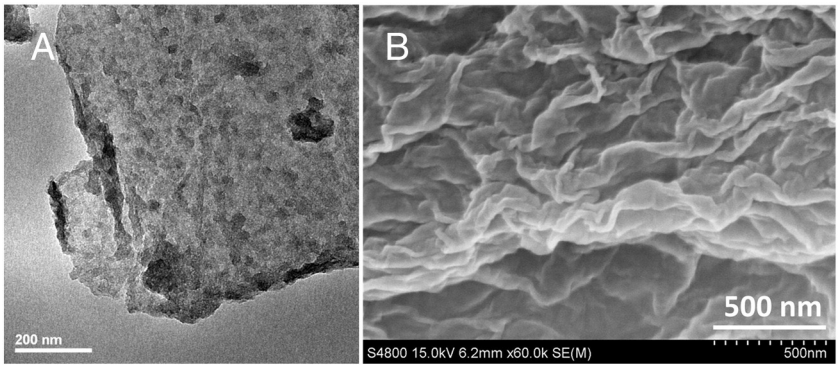

Fig. 2. (A) TEM image and (B) Cross-sectional FESEM images of NiO/GO film.

peak became much stronger. A considerable increment in C/O atomic ratio can be obviously observed in the reduced material (4.16) compared to that of the starting materials (1.92). Considering that the O elemental content shown here includes that in NiO and the O elemental in NiO had no change during the GO deoxygenation, the increase of C/O atomic ratio of NiO/GO composite doesn't change as large as that of pure GO (Usually from 2.54 to 7.87 [27]). Thus it can be speculated that the increment of C/O atomic ratio in graphene should be much higher and deoxygenation of GO is much more significant. The more significant evidence of GO deoxygenation can be obtained from further elemental valence analysis. The C1s high-resolution XPS spectra of NGO-2.0 and NRG-2.0 were performed and the results are shown in Fig. 4B and **C**. From the C1s XPS spectra of NGO-2.0 (Fig. 4B), the four components clearly manifested its fairly high degree of oxidation, corresponding to carbon atoms in different functional groups: the nonoxygenated ring C C═C/C—C (284.8 eV), C—O (hydroxyl and epoxy, 286.3 eV), C═O (carbonyl, 288.2 eV), and O—C═O (carboxyl, 290.1 eV) groups [28–31]. While the C1s XPS spectra of the NRG-2.0 (Fig. 4C) exhibited the same oxygen functionality, their peak intensity confirms an obvious decrease of oxygenated carbon related signals at 286–290 eV. According to the calculation of the integrated areas of the C1s peaks, the non-oxygenated groups of C═C/C—C increase obviously from 51.5% to 60.4%, indicating that successful deoxygenation and partial restoration of the sp^2 carbon sites occurred after CV.

Raman spectroscopy is a non-destructive technique that is widely used to obtain structural information about carbon-based materials [32]. The main features in the Raman spectra of graphitic carbon-based materials are the D and G peaks and their overtones. Structural changes of NGO-2.0 and NRG-2.0 are reflected in their Raman spectra (Fig. 5A). It is found that NGO-2.0 and NRG-2.0 give a similar Raman spectrum in terms of the shapes and positions of Raman peaks. They exhibit a strong D line around 1350 cm^{-1}, representing a breathing mode of κ-point photons of A_{1g} symmetry, and a G line around 1600 cm^{-1}, which should be assigned to the first order scattering of the E_{2g} phonon of sp^2 carbon atoms. However, I_D/I_G of NRG-2.0 (1.17) increases

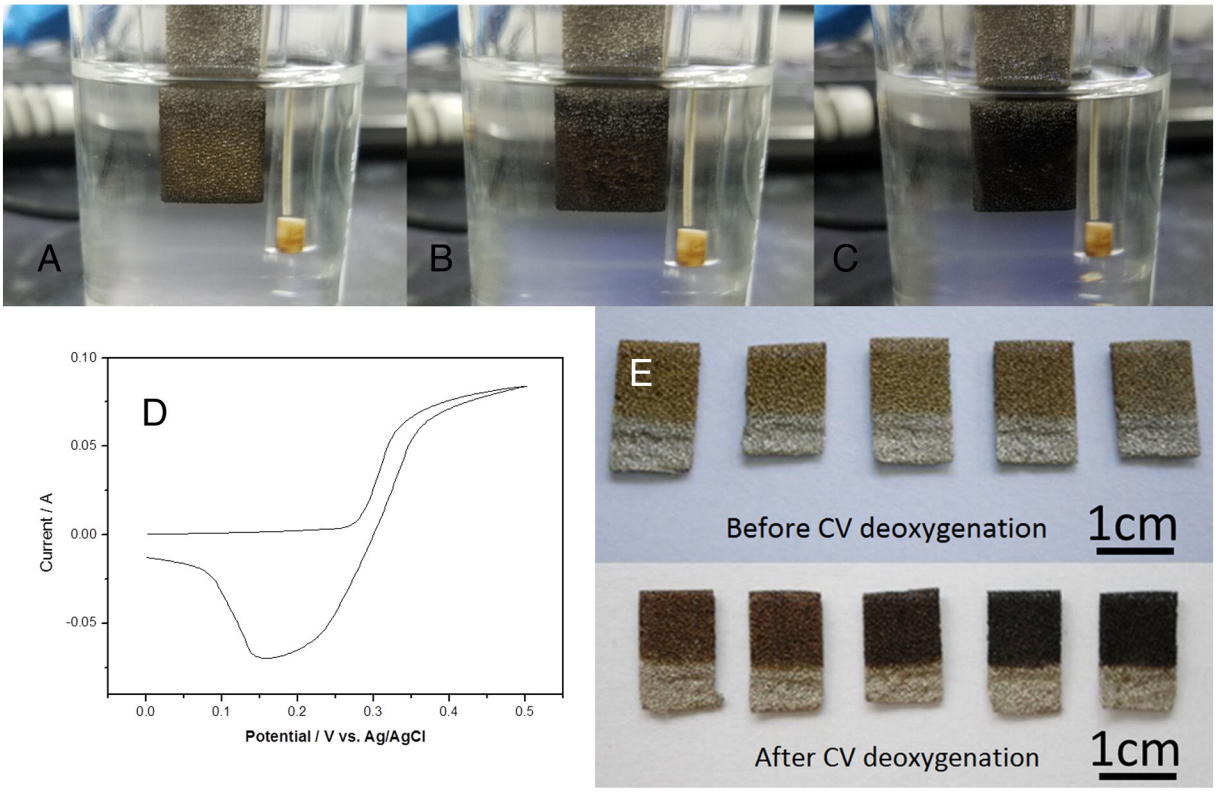

Fig. 3. Images of electrode NGO-2.0 before CV (A), after one CV cycle (B), after five CV cycles (C); First CV cycle of NGO-2.0 (D); Images of all electrodes before and after CV deoxygenation (E).

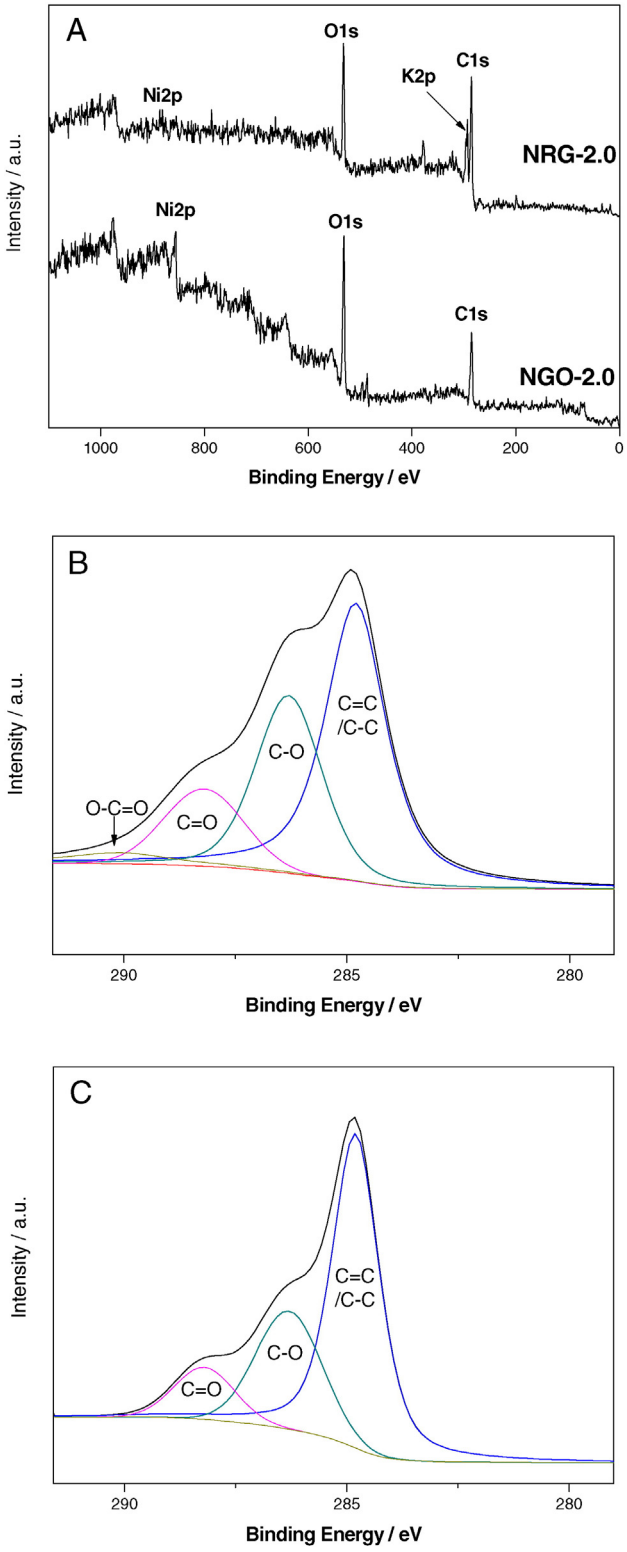

Fig. 4. XPS survey scan spectra (A) and deconvolve XPS C1s Spectra of NGO-2.0 (B) and NRG-2.0 (C).

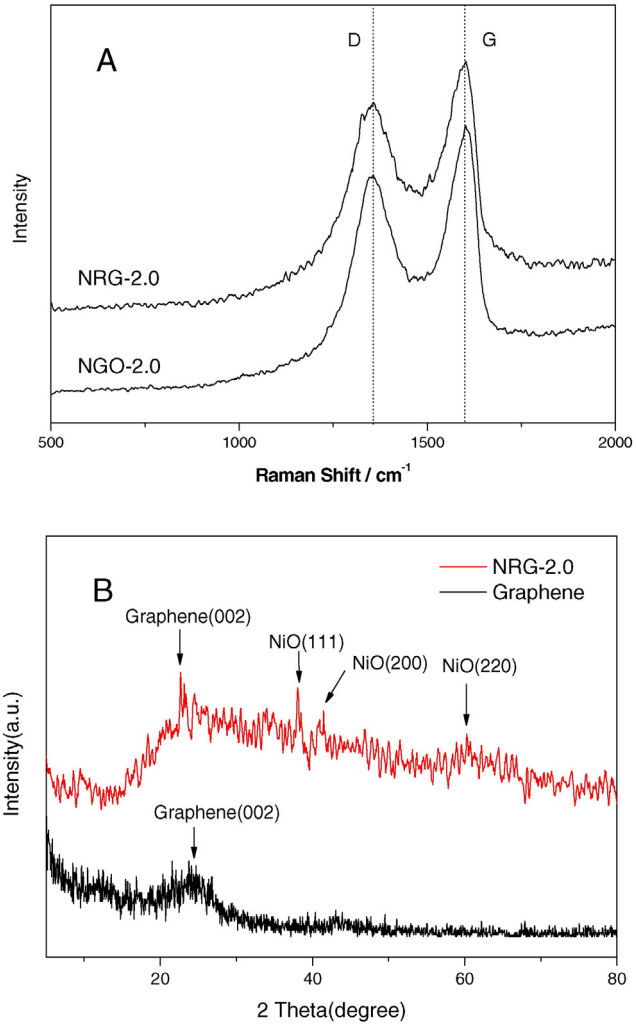

Fig. 5. (A) Raman spectra of NGO-2.0 and NRG-2.0, (B) XRD patterns of Graphene and NRG-2.0.

compared to that in NGO-2.0 (1.02). Many previous literatures reported that the change suggested a decrease in the size of the in-plane sp^2 domains and a partially ordered crystal structure of the graphene, and could be explained if new graphitic domains were created that are smaller in size than the ones present in GO before reduction, but more numerous in number [33,34]. Raman spectroscopy analysis is in good agreement with XPS results.

The final formation of NiO and graphene in NiO/Graphene films can be further confirmed with XRD (Fig. 5B). XRD patterns of NiO/graphene film show peaks at 38.1°, 41.5° and 60.4°, which can be indexed as (111), (220) and (222) crystal planes of a cubic NiO phase, respectively. Additionally, both graphene and the NiO/graphene films show the typical peak (002) for graphene at about 24°. However, 002 peak of NiO/graphene film is at 22.6°, corresponding to d-spacing of about 3.93Å. Meanwhile, 002 peak of graphene film is at 24.4°, corresponding to d-spacing of about 3.65Å. The increased d-spacing suggests that the NiO nanocrystallites affected the re-stacking of the graphene layers during deposition and deoxygenation.

The capacitive behavior of the electrodes was evaluated by CV. All the samples were rejuvenated by CV for five times from 0 to 0.5 V before characterizations to ensure that GO were completely reduced. The CVs of NRG-0.5, NRG-1.0, NRG-1.5, NRG-2.0 and NRG-2.5 are presented in Fig. 6A. All the CVs have two redox reaction peaks which come from the redox reaction between NiO and NiOOH in an alkaline solution shown as follows.

$$NiO + OH^{-1} \rightleftharpoons NiOOH + e^{-1} \quad (1)$$

Through the electrochemical redox reactions, more charges can be stored in the bulk of the nickel oxide. As control, the CV curve of NGO-

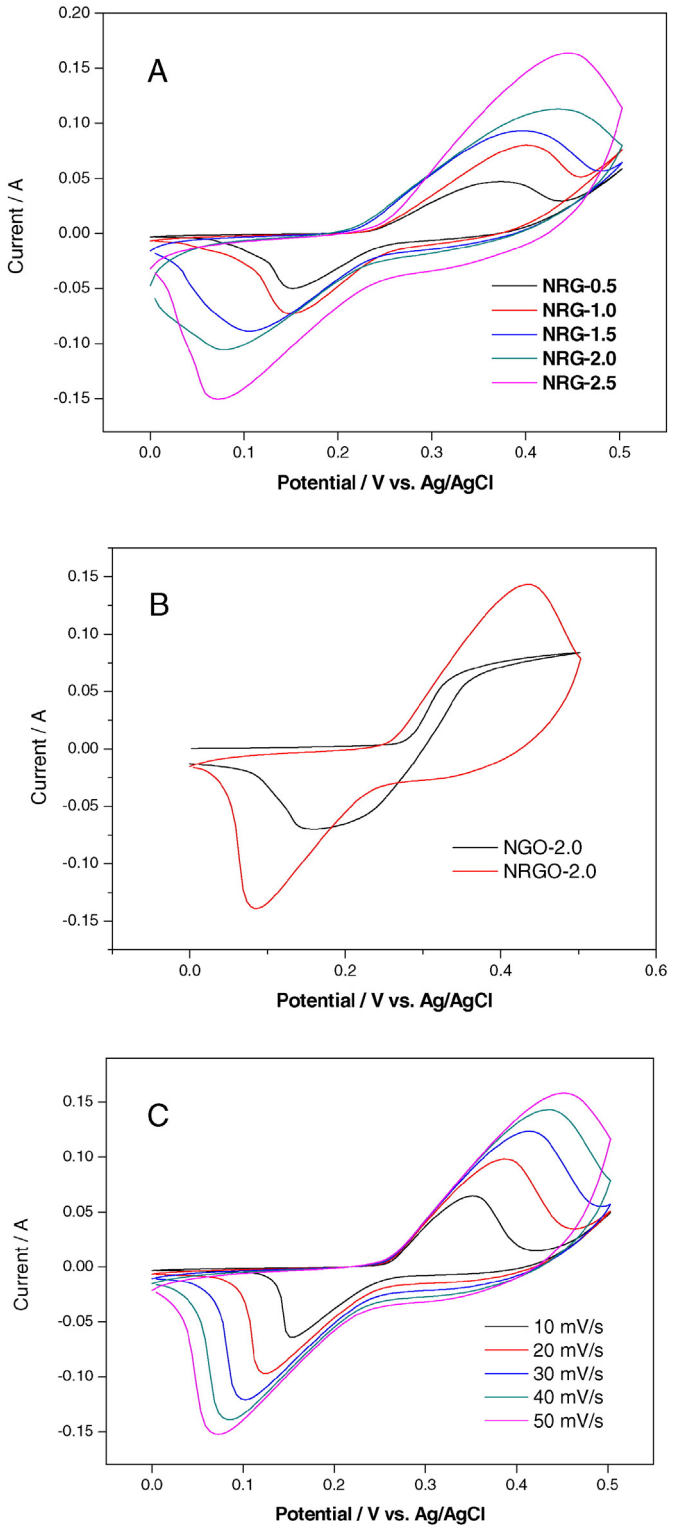

Fig. 6. (A) CVs of electrodes at a scan rate of 50 mV/s; (B) CVs of NGO-2.0 and NRG-2.0; (C) Typical CV curves of NRG-2.0 at different scan rates.

2.0 is also shown in Fig. 6B. Compared with NGO-2.0, NGR-2.0 has larger voltammetric current response revealing higher energy storage. The capacitance is improved due to the presence of pseudocapacitive behavior arising from the reversible Faradaic transitions of Ni(II)/Ni(III). Moreover, the peak currents become much higher from NRG-0.5 to NRG-2.5, which implies that the capacitive performance of the electrodes increases the concentration of Ni^{2+}. This may be due to the increase in NiO content in NiO/graphene electrodes which reveals the pseudocapacitive behavior. At first, we held opinion that there may be a trade-off between the pseudocapacitance and the conductivities. The presence of excess insulated NiO will lead to an increase in the resistance and prevents the output of the current. However, no trade-off was observed in Fig. 6A. With the increase in deposited NiO/Ni, more and more GO was reduced to graphene. Highly conductive graphene acted as the conductive support of the composite electrode. As a result, the conductivity of the electrodes did not decrease, and no trade-off existed from NRG-0.5 to NRG-2.5. The Retention of conductivity can be confirmed by the ΔEp in CV curves. There is on significant change of electrochemical activity with the increase of NiO amount in the electrode. Combination of NiO and graphene results in a high specific capacitance via two charge storage mechanisms: the electric double layer capacitance attributed to the graphene and the pseudocapacitance attributed to NiO [35–37]. NiO can undergo a fast redox reaction to store charge in the bulk of the material and thereby work as a high efficient charge collector. On the other hand, graphene with high current carrying capability and immense specific surface area can support NiO nano structure and release the charge at these reducing potentials. Unfortunately, the preparation of the NiO/GO electrodes with higher content of NiO failed. The suspension for EPD is highly unstable due to the compaction of the electric double layer on GO surfaces if the concentration of Ni^{2+} is more than 2.5 mM. The devices and approaches involved in our method need to be explored. In any event, the strategy of fast fabrication to prepare NiO/graphene composite modified electrodes by EPD is at the stage of being acceptable and points out a new direction for supercapacitor electrode research.

The CVs of NRG-0.5, NRG-1.0, NRG-1.5, NRG-2.0 and NRG-2.5 at different scan rates were measured from 10 to 50 mV/s and a typical curve of NRG-2.0 was shown in Fig. 6C. A pair of redox peaks signifying typical pseudocapacitor behavior was clearly observed in all figures. With the increase of scan rate, the current response increased accordingly, and the oxidation peak potential shifts positively while the deoxidization peak potential shifts negatively. However, no significant change in the shape of CV curve was observed, indicating the good rate property of all electrodes.

The galvanostatic charge-discharge test was conducted to further quantify the specific capacitance of the electrodes. The galvanostatic discharge curves of NRG-0.5, NRG-1.0, NRG-1.5, NRG-2.0 and NRG-2.5 were characterized at various current densities ranging from 5 to 50 A/g and the specific capacitance is calculated according to Eq. (2),

$$C = \frac{2i_m \int Vdt}{V^2 \Big|_{Vi}^{Vf}} \tag{2}$$

where C (F/g) is the specific capacitance, $i_m = I/m$ (A/g) is the current density, where I is the current and m is the active mass of the active materials. $\int Vdt$ is the integral current area, where V is the potential with initial and final values of V_i and V_f, respectively [38]. Fig. 7A shows the typical charge-discharge curves of NRG-2.0 at various current densities ranging from 5 to 50 A/g and Fig. 7B shows the capacitance of all the electrodes at various current densities. From the curves, it can be observed that with the increase in NiO, the discharge time increased, indicating that the capacitive behavior of the electrodes was improved. The result is in good agreement with that of the CV. The specific capacitance of NRG-2.5 can reach as high as 1258 F/g with longest discharge time at the current density of 5 A/g. Furthermore, the specific capacitances of NiO/graphene electrodes changes with the discharge current density. The specific capacitance is 1258, 982, 833, 729, 640, 376 F/g at the current density of 5, 10, 15, 25, 50 A/g, respectively. This may be due to progressively less efficient infiltration of electrolyte into the porous structure at higher current densities, which is a typical shortcoming of the graphene film electrode. Recently, some groups and our team have attempted to control the pore diameter distribution of

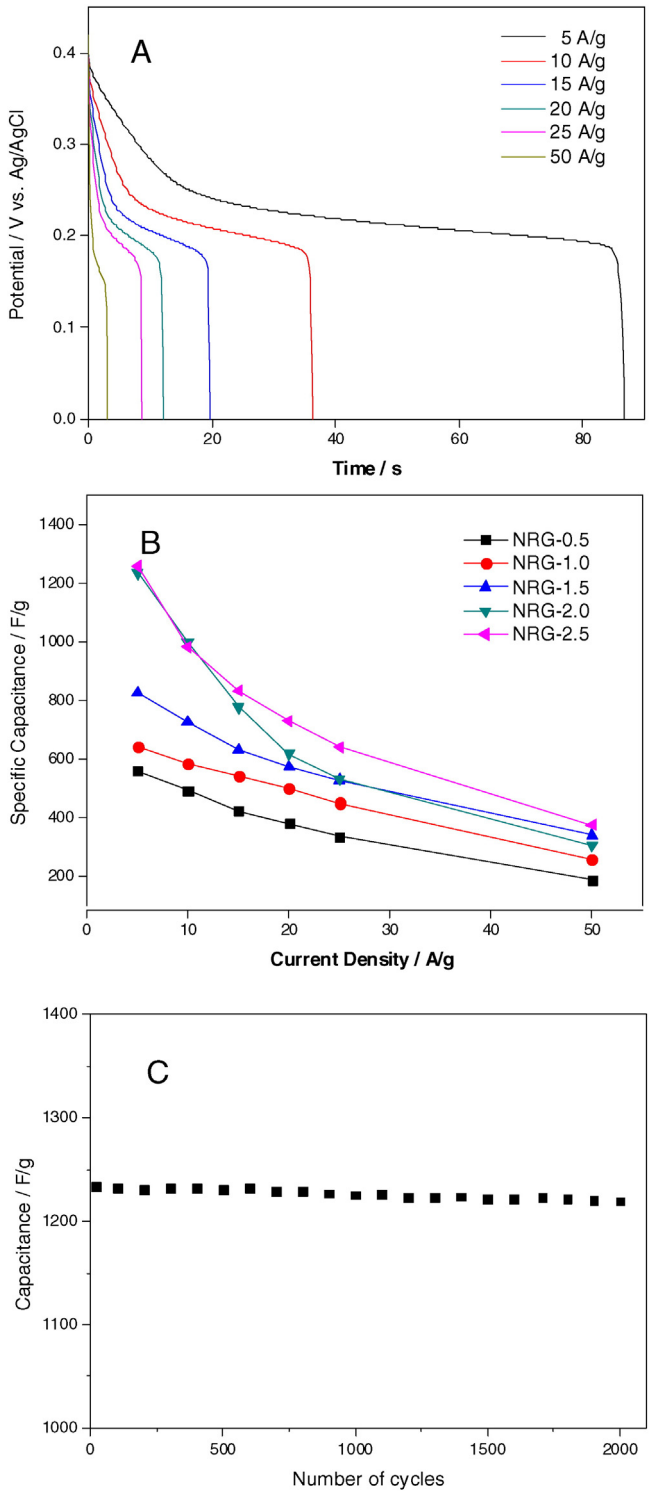

Fig. 7. (A) Typical charge-discharge curves of NRG-2.0 at various current densities ranging from 5 to 50 A/g, (B) Specific capacitance of electrodes at different current densities, (C) Cycling stability of NRG-2.0 electrode at a current density of 5 A/g.

nanomaterials to improve the effective diffusivity [39–41]. However, there is a trade-off between the pore diameter and the mechanical properties. Our investigation herein may give a partial solution to the problem because the NiO-coated GO films have a large interlayer spacing and there are many cavities between interlayer spaces.

As a supercapacitor, the cycle-life stability of electrode is very important for practice use. To evaluate the stability of the electrode, the cycle performance of the NRG-2.0 electrode characterized by the galvanostatic charge/discharge technique at a current density of 5 A/g is displayed in Fig. 7C. On the whole, the as obtained electrode reveals a relatively high capacitance (1234 F/g at 5 A/g) and remarkable cycling stability (98.3% after 2000 cycles). The outstanding cycling stability of this novel NiO/graphene composite electrode demonstrate a successful combination of the advantages of both graphene and NiO nanoparticles, with graphene's contributing to a higher electronic conductivity and porous nano-structure to more active sites for redox reaction at the electrode.

4. Conclusions

In summary, we report a fast fabrication method to prepare NiO/graphene composite film modified electrodes by EPD for supercapacitors. The Ni^{2+}-decorated GO moves towards the cathode (nickel foam) by electric field force. After deposition, the metallic Ni on the as-formed GO films is oxidized to NiO in the drying process and GO can undergo fast deoxygenation to graphene via CV in 6 M KOH aqueous solution. Combination of NiO and graphene results in a high specific capacitance via two charge storage mechanisms: the electric double layer capacitance attributed to the graphene and the pseudocapacitance attributed to NiO. NiO can undergo a fast redox reaction to store charge in the bulk of the material and thereby work as a high efficient charge collector. On the other hand, graphene with the high current carrying capability and immense surface area can support NiO nanostructure and release the charge at these reducing potentials. With the increase in NiO, a highly reduced graphene can be obtained during CV, leading to better capacitive behavior of the electrodes. The highest specific capacitance of the constructed electrodes can reach 1258 F/g at a current density of 5 A/g.

Acknowledgments

The project was supported by the Specialized Research Fund for the Doctoral Program of Higher Education of China (20123219110010) and Priority Academic Program Development of Jiangsu Higher Education Institutions of China (PAPD), partially by NSF Grant of the USA (DMR1231319), NIH/NIDCR Grant of the USA (R01 DE021786), PREM NSF Program Grant (DMR-1205608), and U.S. ARMY Grant (W911NF-15-1-0051).

References

[1] S.J. Patil, C.D. Lokhande, Fabrication and performance evaluation of rare earth lanthanum sulfide film for supercapacitor application: effect of air annealing, Mater. Des. 87 (2015) 939–948.
[2] G. Yu, X. Xie, L. Pan, Z. Bao, Y. Cui, Hybrid nanostructured materials for high-performance electrochemical capacitors, Nano Energy 2 (2013) 213–234.
[3] X. Peng, L. Peng, C. Wu, Y. Xie, Two dimensional nanomaterials for flexible supercapacitors, Chem. Soc. Rev. 43 (2014) 3303–3323.
[4] M. Yang, Y. Zhong, J. Bao, X. Zhou, J. Wei, Z. Zhou, Achieving battery-level energy density by constructing aqueous carbonaceous supercapacitors with hierarchical porous N-rich carbon materials, J. Mater. Chem. A 3 (2015) 11387–11394.
[5] J. Yang, C. Zeng, F. Wei, J. Jiang, K. Chen, S. Lu, Cobalt–carbon derived from zeolitic imidazolate framework on Ni foam as high-performance supercapacitor electrode material, Mater. Des. 83 (2015) 552–556.
[6] H. Xia, C. Hong, B. Li, B. Zhao, Z. Lin, M. Zheng, S.V. Savilov, S.M. Aldoshin, Facile synthesis of hematite quantum-dot/functionalized graphene-sheet composites as advanced anode materials for asymmetric supercapacitors, Adv. Funct. Mater. 25 (2015) 627–635.
[7] R.R. Salunkhe, J. Lin, V. Malgras, S.X. Dou, J.H. Kim, Y. Yamauchi, Large-scale synthesis of coaxial carbon nanotube/$Ni(OH)_2$ composites for asymmetric supercapacitor application, Nano Energy 11 (2015) 211–218.
[8] K. Qiu, Y. Lu, D. Zhang, J. Cheng, H. Yan, J. Xu, X. Liu, J.K. Kim, Y. Luo, Mesoporous, hierarchical core/shell structured $ZnCo_2O_4/MnO_2$ nanocone forests for high-performance supercapacitors, Nano Energy 11 (2015) 687–696.
[9] Y. Zhao, C.A. Wang, Nano-network MnO2/polyaniline composites with enhanced electrochemical properties for supercapacitors, Mater. Des. 97 (2016) 512–518.
[10] M. Wu, Y. Lin, C. Lin, J. Lee, Formation of nano-scaled crevices and spacers in NiO-attached graphene oxide nanosheets for supercapacitors, J. Mater. Chem. 22 (2012) 2442–2448.

[11] B. Dong, H. Zhou, J. Liang, L. Zhang, G. Gao, S. Ding, One-step synthesis of free-standing α-Ni(OH)$_2$ nanosheets on reduced graphene oxide for high-performance supercapacitors, Nanotechnology 25 (2014) 435403–435410.
[12] C.H. Wu, S.X. Deng, H. Wang, Y.X. Sun, J.B. Liu, H. Yan, Preparation of novel three-dimensional NiO/ultrathin derived graphene hybrid for supercapacitor applications, ACS Appl. Mater. Interfaces 6 (2014) 1106–1112.
[13] M. Jing, C. Wang, H. Hou, Z. Wu, Y. Zhu, Y. Yang, X. Jia, Y. Zhang, X. Ji, Ultrafine nickel oxide quantum dots embedded with few-layer exfoliative graphene for an asymmetric supercapacitor: enhanced capacitances by alternating voltage, J. Power Sources 298 (2015) 241–248.
[14] B.Z. Liu, Q. Zhang, H. Wang, Y. Li, Structurally colored carbon fibers with controlled optical properties prepared by a fast and continuous electrophoretic deposition method, Nanoscale 5 (2013) 6917–6922.
[15] M. Wu, Y. Fu, Electrophoretic self-assembly of expanded mesocarbon microbeads with attached nickel nanoparticles as a high-rate electrode for supercapacitors, Nanoscale 6 (2014) 4195–4203.
[16] Q.G. Fu, X.Y. Nan, X. Chen, W.L. Wang, H.J. Li, Y.Y. Li, L.T. Jia, Electrophoretic deposition of SiC nanowires onto carbon/carbon composites to improve the interface bonding of Ti–Ni–Si joint, Mater. Des. 80 (2015) 137–143.
[17] Q. Zheng, Z. Li, J. Yang, J.K. Kim, Graphene oxide-based transparent conductive films, Prog. Mater. Sci. 64 (2014) 200–247.
[18] Y. Li, D. Pan, S. Chen, Q. Wang, G. Pan, T. Wang, In situ polymerization and mechanical, thermal properties of polyurethane/graphene oxide/epoxy nanocomposites, Mater. Des. 47 (2013) 850–856.
[19] P. Song, D. Wen, Z.X. Guo, T. Korakianitis, Oxidation investigation of nickel nanoparticles, Phys. Chem. Chem. Phys. 10 (2008) 5057–5065.
[20] L. Qian, X. Xu, M. Zhang, J. Che, Y. Xiao, Fabrication of NiO-coated single-walled carbon nanotube films on nickel foam as supercapacitor electrodes, Sci. Adv. Mater. 5 (2013) 774–781.
[21] H.L. Guo, X.F. Wang, Q.Y. Qian, F.B. Wang, X.H. Xia, A green approach to the synthesis of graphene nanosheets, ACS Nano 3 (2009) 2653–2659.
[22] G.K. Ramesha, S. Sampath, Electrochemical reduction of oriented graphene oxide films: an in situ Raman spectroelectrochemical study, J. Phys. Chem. C 113 (2009) 7985–7989.
[23] J. Yang, S. Gunasekaran, Electrochemically reduced graphene oxide sheets for use in high performance supercapacitors, Carbon 51 (2013) 36–44.
[24] J.W. Jeon, S.R. Kwon, J.L. Lutkenhaus, Polyaniline nanofiber/electrochemically reduced graphene oxide layer-by-layer electrodes for electrochemical energy storage, J. Mater. Chem. A 3 (2015) 3757–3767.
[25] S. Pei, H.M. Cheng, The reduction of graphene oxide, Carbon 50 (2012) 3210–3228.
[26] T. Kuila, A.K. Mishra, P. Khanra, N.H. Kim, J.H. Lee, Recent advances in the efficient reduction of graphene oxide and its application as energy storage electrode materials, Nanoscale. 5 (2013) 52–71.
[27] J. Che, L. Shen, Y. Xiao, A new approach to fabricate graphene nanosheets in organic medium: combination of reduction and dispersion, J. Mater. Chem. 20 (2010) 1722–1727.
[28] H.K. Jeong, Y.P. Lee, R.J.W.E. Lahaye, M.H. Park, K.H. An, I.J. Kim, C.W. Yang, C.Y. Park, R.S. Ruoff, Y.H. Lee, Evidence of graphitic AB stacking order of graphite oxides, J. Am. Chem. Soc. 130 (2008) 1362–1366.
[29] T. Szabó, O. Berkesi, P. Forgó, K. Josepovits, Y. Sanakis, D. Petridis, I. Dékány, Evolution of surface functional groups in a series of progressively oxidized graphite oxides, Chem. Mater. 18 (2006) 2740–2749.
[30] H.J. Shin, K.K. Kim, A. Benayad, S.M. Yoon, H.K. Park, I.S. Jung, M.H. Jin, H.K. Jeong, J.M. Kim, J.Y. Choi, Y.H. Lee, Efficient reduction of graphite oxide by sodium borohydride and its effect on electrical conductance, Adv. Funct. Mater. 19 (2009) 1987–1992.
[31] S. Liu, J. Ou, J. Wang, X. Liu, S. Yang, A simple two-step electrochemical synthesis of graphene sheets film on the ITO electrode as supercapacitors, J. Appl. Electrochem. 41 (2011) 881–884.
[32] A.C. Ferrari, J. Robertson, Interpretation of Raman spectra of disordered and amorphous carbon, Phys. Rev. B 61 (2000) 14095.
[33] S. Stankovich, D.A. Dikin, R.D. Piner, K.A. Kohlhaas, A. Kleinhammes, Y. Jia, Y. Wu, S.T. Nguyen, R.S. Ruoff, Synthesis of graphene-based nanosheets via chemical reduction of exfoliated graphite oxide, Carbon 45 (2007) 1558–1565.
[34] H. Guo, X. Wang, Q. Qian, F. Wang, X. Xia, A green approach to the synthesis of graphene nanosheets, ACS Nano 3 (2009) 2653–2659.
[35] X. Xia, J. Tu, Y. Mai, R. Chen, X. Wang, C. Gu, X. Zhao, Graphene sheet/porous NiO hybrid film for supercapacitor applications, Chem. Eur. J. 17 (2011) 10898–10905.
[36] Y. Yang, Z. Hu, Z. Zhang, F. Zhang, Y. Zhang, P. Liang, H. Zhang, H. Wu, Reduced graphene oxide–nickel oxide composites with high electrochemical capacitive performance, Mater. Chem. Phys. 133 (2012) 363–368.
[37] P. Cao, L. Wang, Y. Xu, Y. Fu, X. Ma, Facile hydrothermal synthesis of mesoporous nickel oxide/reduced graphene oxide composites for high performance electrochemical supercapacitor, Electrochim. Acta 157 (2015) 359–368.
[38] L. Mai, A. Minhas-Khan, X. Tian, K. Hercule, Y. Zhao, L. Xu, X. Xu, Synergistic interaction between redox-active electrolyte and binder-free functionalized carbon for ultrahigh supercapacitor performance, Nat. Commun. 4 (2013).
[39] M. Ghorbani, F. Nasirpouri, A. Saedi, On the growth sequence of highly ordered nanoporous anodic aluminium oxide, Mater. Des. 27 (2006) 983–988.
[40] Q. Li, Effect of porosity and carbon composition on pore microstructure of magnesium/carbon nanotube composite foams, Mater. Des. 89 (2016) 978–987.
[41] H. Xiao, M. Zhang, Y. Xiao, J. Che, A feasible way for the fabrication of single walled carbon nanotube/polypyrrole composite film with controlled pore size for neural interface, Colloids Surf. B 126 (2015) 138–145.